nature portfolio

https://doi.org/10.1038/s41592-021-01229-w

Supplementary information

Ultrasensitive ultrasound imaging of gene expression with signal unmixing

In the format provided by the authors and unedited

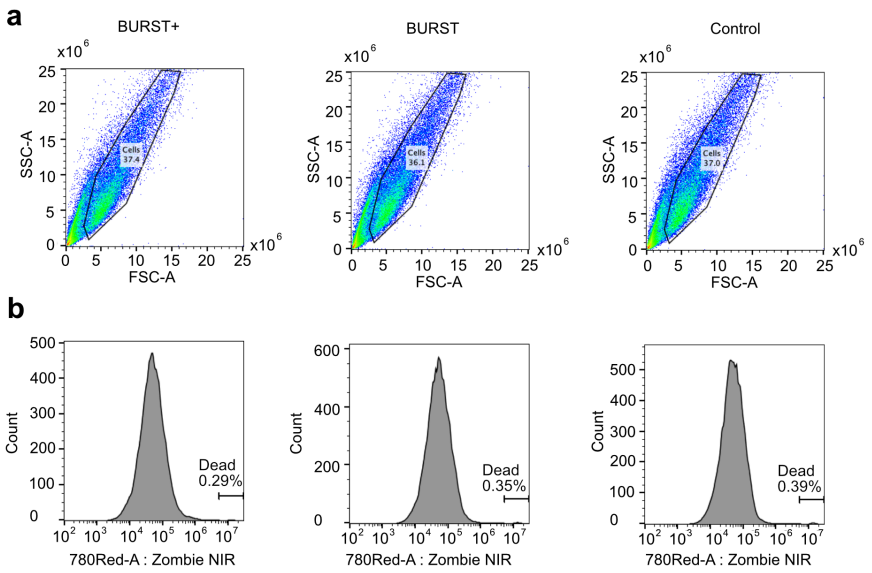

Supplementary Figure 1 | Gating strategy for quantifying cell death in mArg-HEK cells. (**a**) SSC-FSC gating for cell populations exposed to BURST+, BURST, and low-pressure control. (**b**) The corresponding Zombie NIR fluorescence histograms for each population. Cell death was quantified by gating the fraction of cells that emitted Zombie NIR fluorescence. The cutoff was the same for all samples.

Supplementary Note 1: Collapse signal generation mechanism

In performing the single cell detection experiments, we observed that the BURST signals from single cells tended to fall into two distinct categories: small, point-like "dim" signals of moderate intensity between 20 dB and 60 dB, and larger, elongated "bright" signals with intensities of 60 dB to 80 dB (**Fig. 6, b, e**). Analysis of the signal intensity distributions for BURST and BURST+ applied to cells in liquid suspension revealed that BURST generated predominantly dim signals (**Extended Data Fig. 2a**) and that BURST+ generated predominantly bright signals, though dim signals were also present (**Extended Data Fig. 2b**). An understanding of the mechanisms behind these acoustic phenomena would allow us to better predict the performance of BURST and BURST+ in novel settings.

As a starting point for investigation, we hypothesized three mechanisms by which acoustic collapse of GVs might result in strong, transient ultrasound signal: 1) the same linear scattering that creates contrast when imaging below the collapse threshold of the GV, 2) an acoustic wave generated by the rapid volume change that occurs during GV collapse, or 3) cavitation of nanobubbles liberated from the GVs following collapse. In the case of (1), the signal strength is due to an increase in scattering amplitude in proportion to the higher pressures applied, while the signal transience is explained by collapse of the GVs after the initial scattering event. For (3), signal transience would result from the sub-millisecond dissolution times of the nanobubbles.

To test these hypotheses, we imaged ARG Nissle in liquid buffer suspension at 10^3 cells/ml with a range of pulse sequences differing in pressure level, number of waveform cycles, and frame rate. We used the same setup and sample preparation protocol used for the single cell detection experiments. We first applied a pressure ramp with BURST and BURST+ to determine the pressure threshold at which different signal intensities are generated for

each pulse sequence. Dim signals appeared in the BURST images at 3.7 MPa, but remained very sparse up to 3.9 MPa (**Extended Data Fig. 2c**). Bright signals did not appear in any BURST images. Both dim signals and bright signals appeared in BURST+ images at 3.4 MPa, although bright signals were very sparse, with less than one per frame at this pressure. Bright signals appeared consistently in BURST+ frames at 3.9 MPa and gradually increased in number at higher pressures (**Extended Data Fig. 2d**). Since BURST and BURST+ have identical pressure maxima and minima, these results suggest the larger number of cycles in BURST+ is necessary for the generation of bright signals and increases the generation of dim signals. Interestingly, although the 50% acoustic collapse pressure threshold of GVs expressed in ARG Nissle is 2.5 MPa, neither pulse sequence generated observable signal at 2.8 MPa. One explanation for this is that GV collapse is a stochastic event that occurs with probability proportional to both PPP and duration of insonation. However, both bright and dim signals are only observed in the first collapse frame for all pressure levels, which suggests that all GVs in the field of view collapse after the first pulse but, depending on the pulse parameters and GV characteristics, may not generate signal. This suggests that mechanism (2) is unlikely for bright or dim signals since it predicts that GV collapse is a sufficient condition for signal generation.

Although both bright and dim signals increased in number at higher pressures (**Extended Data Fig. 2c-d**), the peak intensity of the bright signals increased in direct proportion to the increase in pressure (**Extended Data Fig. 2e**). The number of dim signals, in contrast, increased with pressure while their intensity remained relatively constant up to 4.1 MPa. If the dim signals were generated by mechanism (1), we would expect to observe the opposite: there should be scattering from all cells in the field of view at an intensity that increases proportionally with incident pressure. Instead, our observations are consistent with a stochastic collapse model in which GVs in a given cell generate collapse signal with a probability proportional to the peak positive acoustic pressure. The stochasticity may be intrinsic to the physical process of collapse or may result from variability in shape, size, and number of expressed GVs. In either case, we may rule out mechanism (1) for both bright and dim signals. The evidence thus far suggests that both the bright and dim signals are generated from mechanism (3): the interaction of liberated nanobubbles with the high-pressure acoustic waveform. However, this does not explain their markedly different characteristics.

To investigate the temporal properties of the bright and dim signals, we designed an ultrafast implementation of BURST+ with an inter-frame delay of 100 μsec. Although both bright and dim signals appear transient in the standard BURST+ pulse sequence with an inter-frame delay on the order of 10 msec, the ultrafast sequence showed that many bright signals persist after several high-pressure transmits (**Extended Data Fig. 2f**). In contrast, the band of dim signals always vanishes after the first high-pressure frame. Because mechanisms (1) and (2) depend on an irreversible collapse of the GV shell, this provides further evidence against their involvement in generation of the bright signals.

To obtain a tighter upper bound on the persistence time of the dim signals, we applied a cycle ramp with numbers of cycles ranging from 1 to 12. We held PPP constant at 4.0 MPa for each pulse sequence since this pressure level maximized visibility of individual bright and dim sources in the same frame. Both the intensity and size of the

bright signals increased in proportion to the number of cycles (**Extended Data Fig. 2g-h**) Interestingly, after 2 cycles, more cycles did not obviously increase the number of either bright or dim signals (**Extended Data Fig. 2g**), suggesting a regime change in the signal generation mechanism caused by the presence of more than one cycle. The size of the dim signals, in contrast, did not change with the number of cycles, remaining at approximately the size of 1 wavelength (250 μm in this case). This implies that if the dim sources are generated by microbubbles, their dissolution times must be less than 500 nsec.

Physical modeling of GV collapse and nanobubble nucleation, dissolution, and cavitation will likely be required to elucidate the differences between the bright and dim signal generation mechanisms. While such modeling is beyond the scope of this work, we propose here a qualitative model that may account for our observations. It has been shown that, when insonated at 5 MHz with PPP > 4 MPa, microbubbles below a threshold radius of 800 nm decay as $1/R^6$ while larger bubbles undergo resonance enhancement[3], increasing in size through rectified diffusion. Under this proposed mechanism, all nanobubbles liberated by the first positive half-cycle initially have radii below the 800 nm decay threshold, as predicted by typical GV volume[4]. During the first negative half-cycle, rarefaction of these nanobubbles generates the dim signals and also generates bubbles with radii above the decay threshold due to rectified diffusion or coalescence of the nanobubbles. In the case of multi-cycle waveforms, subsequent cycles result in cavitation of the larger bubbles, which generates the bright signals (**Extended Data Fig. 2i**). In contrast, single-cycle waveforms do not generate bright signals because there are no subsequent cycles to cavitate the larger bubbles that form following the first negative half-cycle (**Extended Data Fig. 2j**). In this case, the dim signals generated by multi-cycle waveforms would be due to nanobubbles that remain below the decay threshold following the first negative half cycle.

We present an example of how differences in the punctate signals generated by BURST and BURST+ (**Extended Data Fig. 2k)** are reflected in the RF waveforms of the individual low- and high-pressure frames in **Extended Data Fig. 2, l-n.** As expected from the dB-scale images, the punctate BURST+ signal is significantly higher in intensity and longer in duration. To illustrate aggregate trends in RF waveform shape and intensity for BURST and BURST+ signals, we plotted RF waveforms aligned by the location of peak intensity of their envelope (**Extended Data Fig. 2, o-q**). Because a bimodal distribution of punctate signals is present in BURST+ images, we plotted separately the aligned waveforms for bright BURST+ signals (**Extended Data Fig. 2p**) and dim BURST+ signals (**Extended Data Fig. 2q**). Based on the thresholds shown in **Extended Data Fig. 2a, b**, we defined dim sources as those with peak intensities between 20 dB and 60 dB and bright sources as those with peak intensities between 60 dB and 80 dB. Comparing the bright BURST+ signals to the BURST signals, we see that the greater intensity and duration of the bright BURST+ signals is fairly consistent. The phase and frequency of both BURST and bright BURST+ signals are also consistent, as evidenced by the clear average waveform shape that emerges from both alignments. Interestingly, the dim BURST+ signals are slightly lower in intensity than the dim BURST signals. This may be due to a selection effect in which larger nanobubbles that would produce higher-intensity dim signals with BURST instead produce bright signals with BURST+.

To investigate the differences in effective axial resolution for BURST and BURST+, we measured the full width at half maximum (FWHM) of the envelopes corresponding to these three categories of RF waveform. The FWHM of the dim BURST punctate signals is 0.20 ± 0.18 mm, the FWHM of the dim BURST+ punctate signals is 0.35 ± 0.37 mm, and the FWHM for the bright BURST+ punctate signals is 1.3 ± 0.42 mm (**Extended Data Fig. 2r**). For linear scatters, we would expect the BURST+ transmit waveform to result in a threefold lower axial resolution than BURST because it uses three times the number of cycles. In fact, the FWHM of the bright BURST+ signals is even larger, suggesting that ringdown due to inertia of the cavitating nanobubbles may cause them to continue to generate pressure waves after they have stopped being driven by the transmitted waveform.

References

1. Chen, W.-S., Matula, T. J. & Crum, L. A. The disappearance of ultrasound contrast bubbles: Observations of bubble dissolution and cavitation nucleation. *Ultrasound in medicine & biology* **28**, 793–803 (2002).
2. Lakshmanan, A. *et al.* Preparation of biogenic gas vesicle nanostructures for use as contrast agents for ultrasound and MRI. *Nature Protocols* **12**, 2050–2080 (2017).